PERGAMON

International Journal of Heat and Mass Transfer 45 (2002) 3987–3996

International Journal of HEAT and MASS TRANSFER

www.elsevier.com/locate/ijhmt

Non-heating simulation of pool-boiling critical heat flux

Yong-Hoon Jeong [a], Won-Pil Baek [b,1], Soon Heung Chang [a,*]

[a] *Department of Nuclear and Quantum Engineering, Korea Advanced Institute of Science and Technology, 373-1 Guseong-dong, Yuseong-gu, Daejeon 305-701, South Korea*

[b] *Korea Atomic Energy Research Institute, P.O. Box 105, Yuseong, Daejeon 305-600, South Korea*

Received 4 October 2000; received in revised form 23 February 2002

Abstract

This paper presents a non-heating experimental method that simulates the critical heat flux (CHF) phenomenon in pool boiling. In the experiments, with providing controlled air flow through the holes on a plate submerged in a pool of water, the liquid sublayer (macrolayer) thickness and bubble departure frequency have been successfully measured by a conductance probe. The CHF is reasonably predicted by applying the measured parameters to a liquid macrolayer dryout model. The measured trends of the macrolayer thickness and bubble departure frequency with air mass flux are also consistent with the present understanding. As a result of this experimental study, it is expected that the non-heating method would be useful to investigate the various parametric effects on pool and flow boiling CHF, with avoiding the difficulty in heating and large electric power requirement even for complex geometries.

1. Introduction

The critical heat flux (CHF) is an important thermal-hydraulic phenomenon that should be considered in designing and operating various heat transfer units including nuclear reactors, fossil-fuel boilers, electronic chips, etc. A significant amount of work has been performed over the last four decades to identify physical mechanisms leading to the CHF, to obtain reliable prediction models, and to develop enhancement techniques. However, understanding of the phenomenon is still insufficient in the aspects of detailed CHF mechanisms, effects of various parameters, prediction models applicable to wide range of conditions, etc.

One of the reasons for insufficient understanding is the difficulty in conducting CHF tests for complex geometry and/or high heat fluxes. Because the required heat flux should be supplied to test sections by direct or indirect electrical heating, the CHF of complex or large structures has not been investigated in detail. The non-heating simulation of CHF conditions is examined in this work to resolve this situation.

In developing the non-heating method for pool-boiling CHF, the liquid macrolayer (sublayer) dryout mechanism is assumed as the fundamental CHF mechanism. It has been suggested by several investigators as one of the most probable mechanisms of CHF occurrence. The model assumes periodic growth and departure of a vapor clot on the heated surface and the existence of a liquid macrolayer between the heated surface and the vapor clot. The CHF is postulated to occur when the liquid in the macrolayer is depleted by evaporation during the growth of a large vapor clot. Therefore, the main parameters determining the CHF are the initial macrolayer thickness and bubble departure frequency. If we know these two values, we can calculate the corresponding CHF value.

Previous experiments by Gaertner and Westwater [3], Gaertner [4], Katto and Yokoya [8], and Bhat et al. [1] support the presence of the macrolayer under the vapor clot on the heater surface. Based on these observations, Haramura and Katto [5] suggested a macrolayer dryout model for prediction of pool-boiling CHF. They assume

* Corresponding author. Tel.: +82-42-869-3816; fax: +82-42-869-3810.

E-mail addresses: wpbaek@kaeri.re.kr (W.-P. Baek), shchang@mail.kaist.ac.kr (S.H. Chang).

[1] Tel.: +82-42-868-8913; fax: +82-42-868-8362.

0017-9310/02/$ - see front matter
PII: S0017-9310(02)00100-X

Nomenclature

A_v	total bottom area of vapor stems (m^2)	ρ_g	vapor density (kg/m^3)
A_w	surface area of heater (m^2)	ρ_l	liquid density (kg/m^3)
d_c	cavity mouth diameter (m)	$\Delta\rho$	density difference between liquid and gas (kg/m^3)
f	detachment frequency (Hz)	σ	surface tension (N/m)
h_{fg}	heat of vaporization (J/kg K)	μ	viscosity of liquid
N	active nucleation density (sites/m^2 or sites/m)	*Subscripts*	
T_{sat}	saturation temperature (K)	f	liquid
ΔT	wall superheat (K)	g	vapor
q_{CHF}	critical heat flux (W/m^2)		
δ_l	initial macrolayer thickness (m)		
ϕ	contact angle between heater surface and bubble (–)		

that the CHF occurs when the macrolayer is depleted before the detachment of overlying vapor bubble or bubbles:

$$q_{CHF} = \delta_l \rho_l h_{fg}(1 - A_v/A_w)f \quad (1)$$

where f is the detachment frequency, δ_l the initial macrolayer thickness, A_w the surface area of the heater, and A_v the total bottom area of vapor stems.

Several researchers have tried to measure the macrolayer thickness. Gaertner and Westwater [3] observed macrolayers using an upward-facing horizontal disk of 50 mm diameter and discussed the relationship between the macrolayer thickness and the diameter of vapor stems in the macrolayer. After him, considerable measurements have been performed using conduction probes. In most experiments, the interface of macrolayer is determined by the position where the void fraction or bubble frequency changes drastically. From the heater wall to the macrolayer boundary, void fraction and fluctuation frequency are nearly constant. Near the boundary, the void fraction increases drastically while the fluctuation frequency decreases drastically. From these evidences, they determined the macrolayer thickness.

In this study, the liquid macrolayer thickness and bubble departure frequency are measured by a conductance probe while providing controlled air flow through the holes on a plate submerged in a pool of water. The feasibility of the non-heating simulation is validated by applying the measured parameters to Eq. (1) and comparing the results with the well-known CHF values. The effects of the air mass flux on the macrolayer thickness and the bubble departure frequency are also compared with the previous understanding reported by others. This paper also discusses future possible applications of the non-heating method.

2. Experimental method

Fig. 1 shows a schematic of the experimental apparatus used in this study. The air-blowing surface is made of a copper plate of 50 mm where the diameter of the actual air-blowing area is varied from 25 to 40 mm. Nucleation sites are modeled by the small holes of 0.3 or

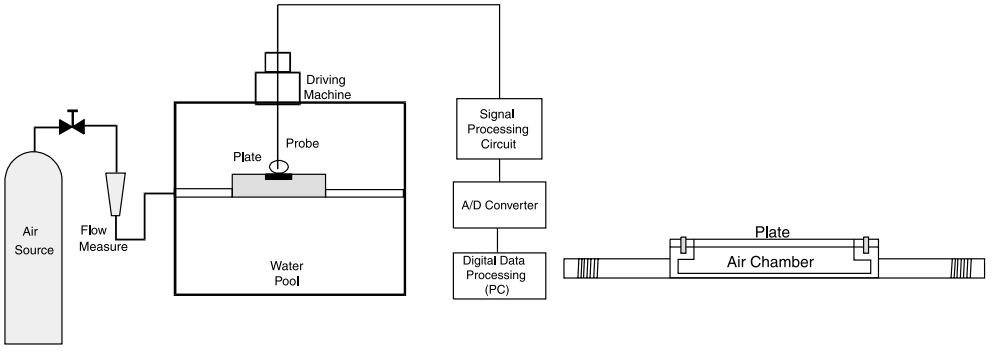

Fig. 1. Schematic diagram of the experimental apparatus.

Table 1
Summary of experimental conditions

Test number	Disk diameter (mm)	Hole pitch (mm)	Hole diameter (mm)	Array
I	25	1.0	0.3	Square
II	30	1.0	0.3	Square
III	40	1.0	0.3	Square
IV	30	1.0	0.2	Square
V	30	1.0	0.2	Triangle
VI	30	1.5	0.2	Square

0.2 mm diameter, arranged with a pitch of 1 or 1.5 mm with square and triangular array. Experimental conditions are summarized in Table 1.

The correlations for active nucleation site density by Wang and Dhir [11] and Paul and Abdel-Khalik [9] are used to determine the number density of holes. Wang and Dhir [11] correlated their data of active nucleation site density as a function of the wall superheat and contact angle as follows:

$$N = 5 \times 10^{-27}(1 - \cos\phi)/d_c^6 \tag{2}$$

where the cavity mouth diameter d_c is a function of the local superheating:

$$d_c = \frac{4\sigma T_{sat}}{\rho_g h_{fg} \Delta T} \tag{3}$$

For water under atmospheric pressure, the contact angle is about 85°, and the wall superheat is about 10–20 °C. So, the active nucleation site density would be in the range of 60,000–4,000,000 sites/m^2 or 250–2000 sites/m [2]. In other words, the pitch between active nucleation site would be 0.5–4.0 mm. On the other hand, Abdel-Khalik's correlation is given as follows [9]:

$$N = 1.207 \times 10^{-3} q + 15.74 \tag{4}$$

This represents the active nucleation site density of ~1585 sites/m for the CHF value of ~1300 kW/m^2 that is expected on the flat plate. The pitch between active nucleation sites would be ~0.6 mm. The pitch of 1 mm between drilled holes was determined based on the above considerations.

The heat flux condition was simulated by controlling the air-flow rate. Here, the heat flux q'' corresponds to the air-flow rate $\dot{V}$ as follows:

$$q''A = \dot{V}\rho_g h_{fg} \tag{5}$$

Air bubbles from the plate coalesce together and form large air mushrooms like vapor mushrooms in heating experiment (Fig. 2). As the air-flow rate increases, the size of air mushroom increases together. Generally, the behavior and appearance of air bubbles and mushroom are very similar with those of vapor.

The void fraction was measured at various distances from the drilled plate by a conduction probe. The schematic of the conduction probe is shown in Fig. 3. The probe tip, the maximum diameter of which is 0.075 mm, is canned by two of steel cans. The gaps between the tip and supporting cans are filled with epoxy and Teflon so that the tip and cans are electrically insulated.

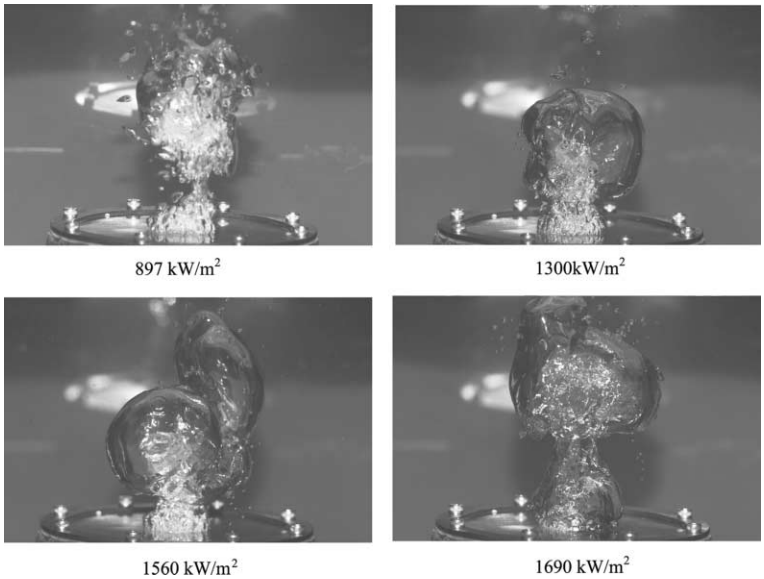

Fig. 2. Air bubble on simulated heater plate.

Fig. 3. Schematic diagram of conduction probe.

If the probe tip is contacted with water, the current path between the tip and outer can is established with generating voltage signals in the range of 3.0–5.0 V. If the tip is contacted with air bubbles, the current path becomes open and the voltage signal is dropped to a low value.

This voltage signals are gathered by using an A/D converter and a PC with an adequate data acquisition program (Fig. 1). A typical voltage signal is illustrated in Fig. 4. Generally, in this study, the voltage signal varied between 1.0 and 3.5 V. For further analysis, we have to determine a cut-off voltage that divides air and water phases. Determination of the cut-off voltage usually requires a calibration based on the knowledge of the actual void fraction. However, in this study, we do not need to measure the exact value of void fraction; instead, we examined the difference in the pattern (relative value) of void fraction distribution between the liquid macrolayer and the air bubble. Several cut-off voltages were tested as illustrated in Fig. 5, resulting in an appropriate cut-off voltage of 2.25 V. The relative void fraction distribution could be measured reliably with this value.

For given air-blowing area and air-flow rate, the void fraction distributions were measured at various distances between 0.02 and 30.0 mm from the drilled plate by changing the location of the conduction probe.

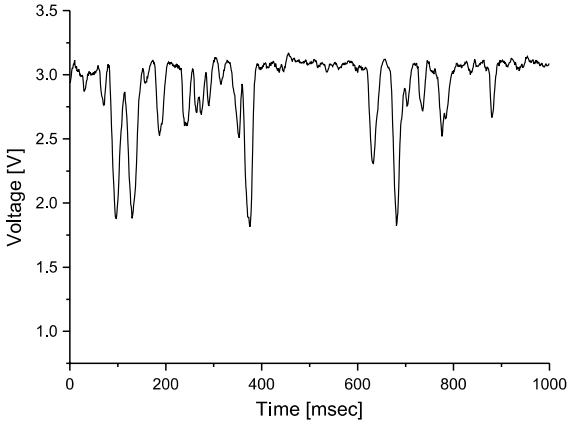

Fig. 4. Sample voltage signal from conduction probe.

3. Results and discussion

3.1. Measurement of the macrolayer thickness

The measured distribution of void fraction for the disk of 25 mm diameter (air-blowing area) is shown in Fig. 6. The void fraction (time-averaged resistance) is nearly constant and low near the wall, but sharply increases in the distance of 0.1–0.5 mm. The first transition points of the void fraction, which can be considered as the macrolayer thickness, are located in the range of 0.1–0.2 mm. Figs. 7–11 show that the void fraction distributions are very consistent even in different air-blowing areas, pitches (nucleation site density), hole diameters and arrays of holes (nucleation site). Therefore, the macrolayer thickness can be determined based on the void fraction distribution as in this work.

The major contributor to the macrolayer thicknesses measured from this study under various conditions (see Table 1) is air-blowing rate (heat flux). And, the other parameters, such as hole diameter, disk diameter, pitch between holes, array formation cannot give much effects on macrolayer thickness.

Several researchers have measured the macrolayer thickness in actual boiling of water on horizontally upward-facing plates using various measuring devices and suggested some experimental or theoretical correlations [3,5,7,10]. Their correlations and the results of the present work are compared in Fig. 12. It is noted that non-boiling experimental results in this work agree reasonably well with previous heating experiments, in particular considering the difference between steam and air properties.

3.2. Measurement of the bubble departure frequency

The bubble departure frequency of flat disks has been measured by the conductance probe. It can be obtained by analyzing the signals from the conductance probe located at a sufficiently long distance from the air-blowing surface ($x > 50$ mm) as the vapor mushroom (clot) on the air-blowing surface is smaller than 50 mm. The measured bubble departure frequency according to various heat flux is shown in Fig. 13. Some of the measured frequencies were confirmed by the high-speed camera recordings.

Haramura and Katto [6] derived a correlation for the hovering period of vapor mass τ_d as:

$$\tau_d = (3/4\pi)^{1/5}\{4[(11/16)\rho_l + \rho_v]/[g(\rho_l - \rho_v)]\}^{3/5} v_l^{1/5} \quad (6)$$

where v_l is the vapor volume generation rate per unit heater area. Because the vapor volume generation rate is

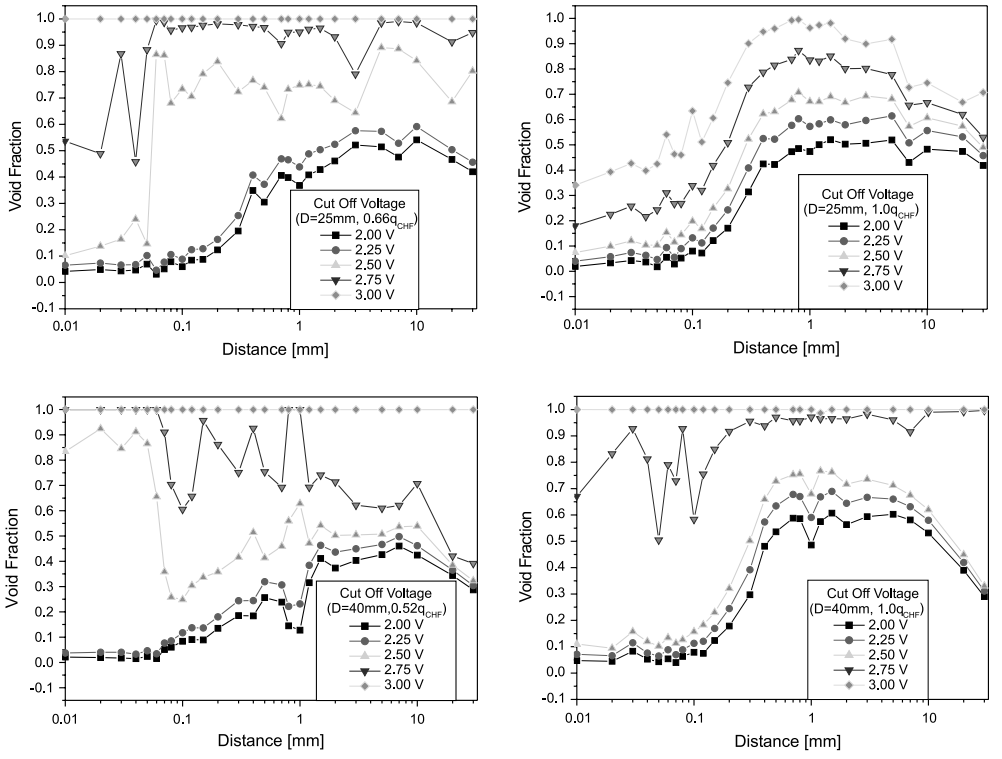

Fig. 5. Determination of cut-off voltage.

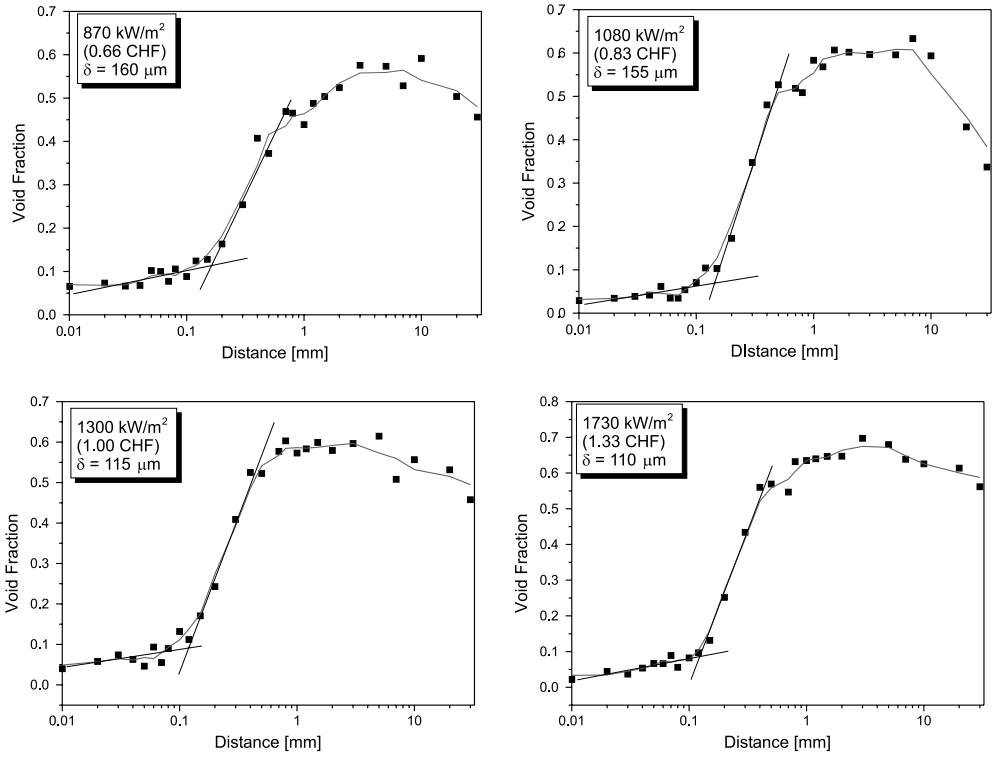

Fig. 6. Void fraction distribution ($D = 25$ mm, $P = 1.0$ mm, H (hole diameter) $= 0.3$ mm, square array).

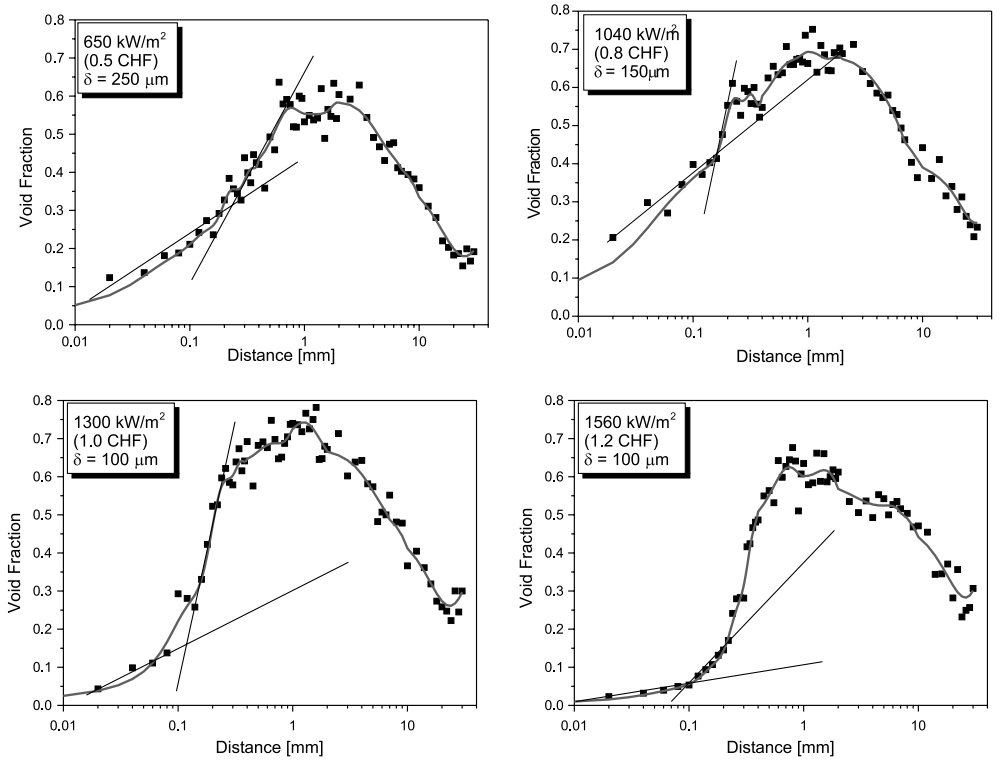

Fig. 7. Void fraction distribution ($D = 30$ mm, $P = 1.0$ mm, $H = 0.3$ mm, square array).

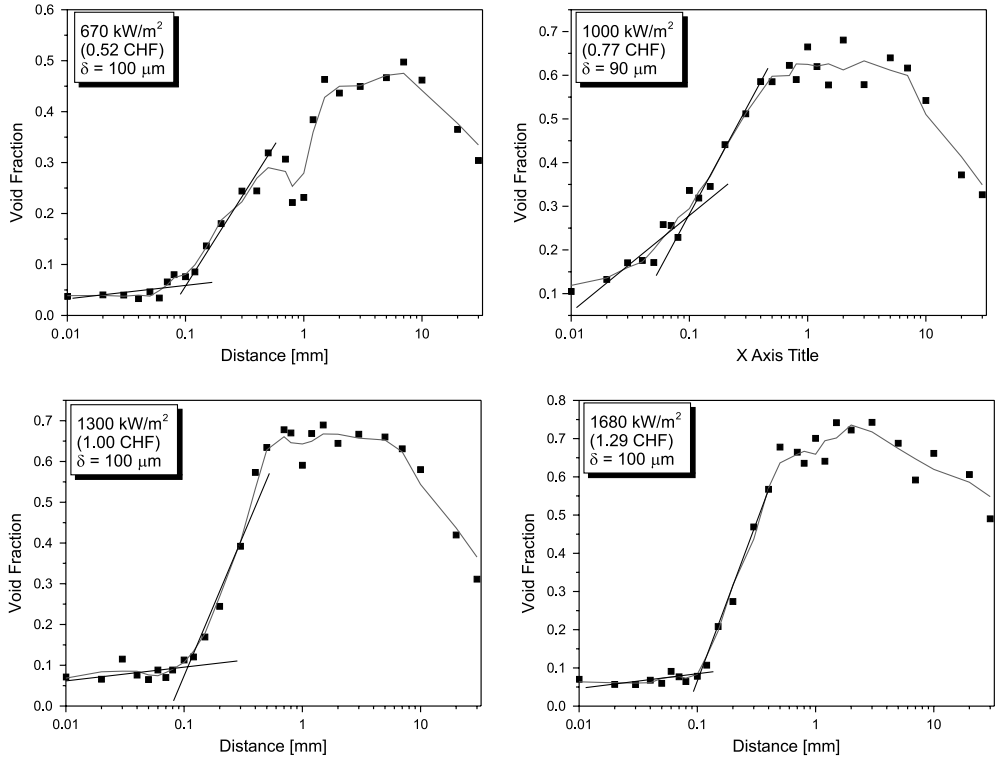

Fig. 8. Void fraction distribution ($D = 40$ mm, $P = 1.0$ mm, $H = 0.3$ mm, square array).

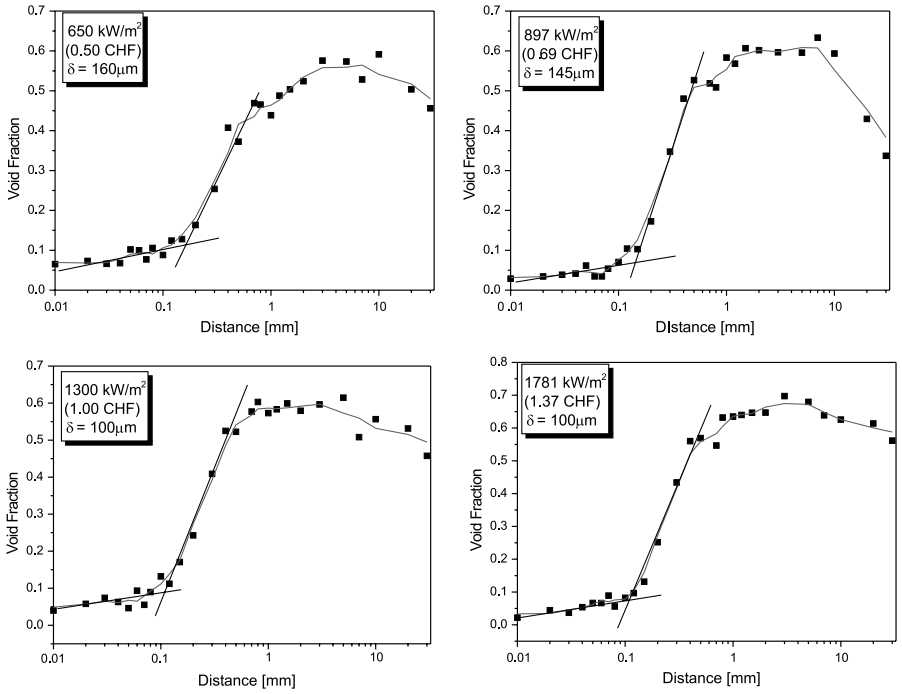

Fig. 9. Void fraction distribution ($D = 30$ mm, $P = 1.0$ mm, $H = 0.2$ mm, square array).

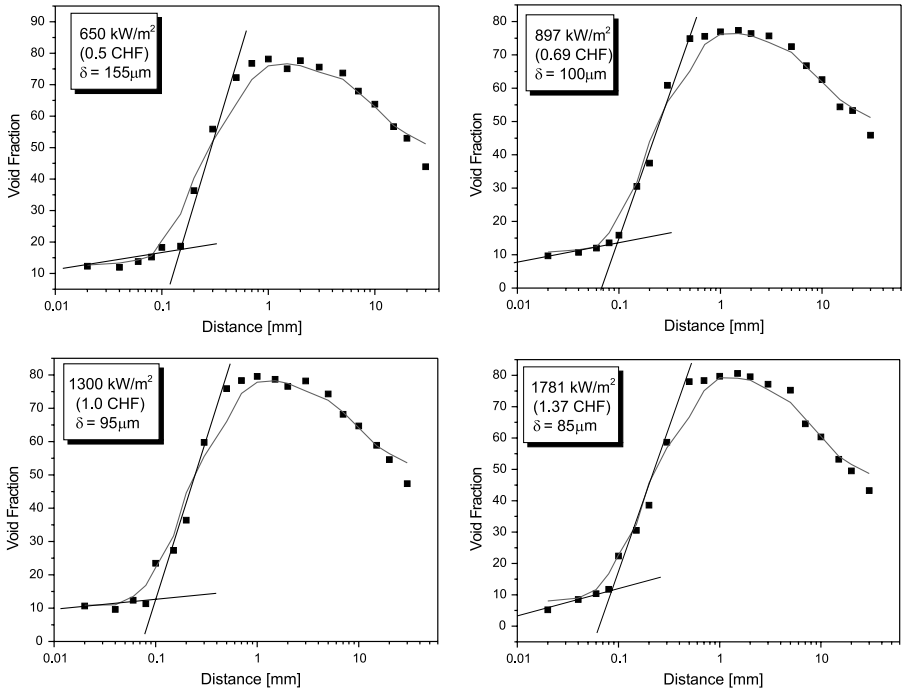

Fig. 10. Void fraction distribution ($D = 30$ mm, $P = 1.0$ mm, $H = 0.2$ mm, triangular array).

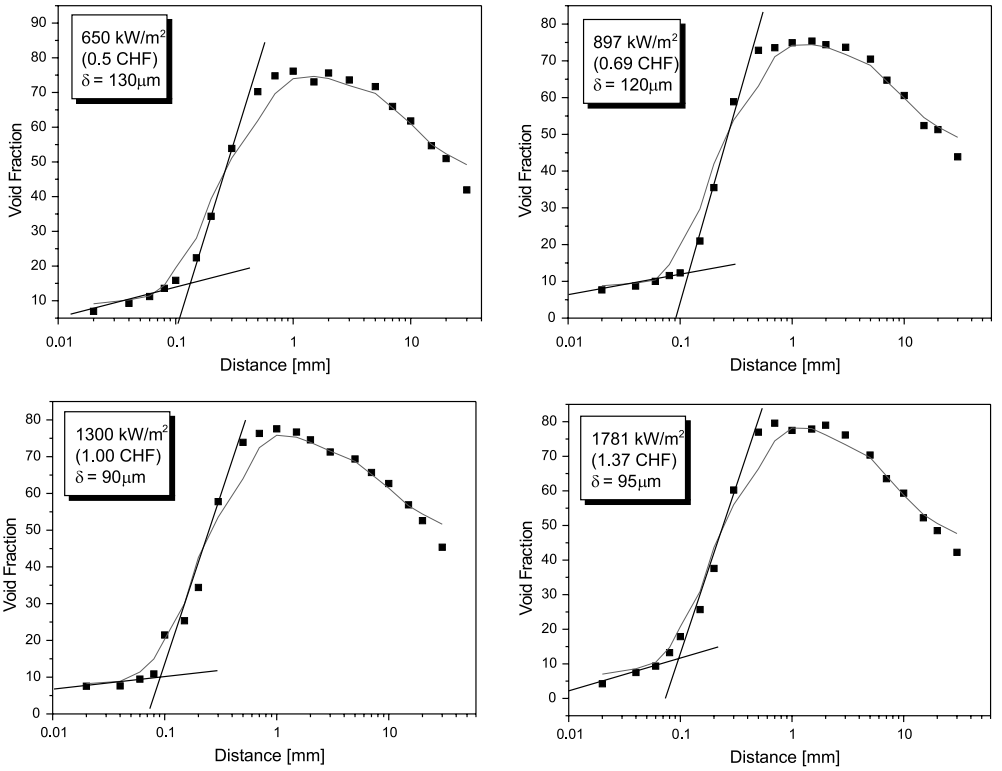

Fig. 11. Void fraction distribution ($D = 30$ mm, $P = 1.5$ mm, $H = 0.2$ mm, square array).

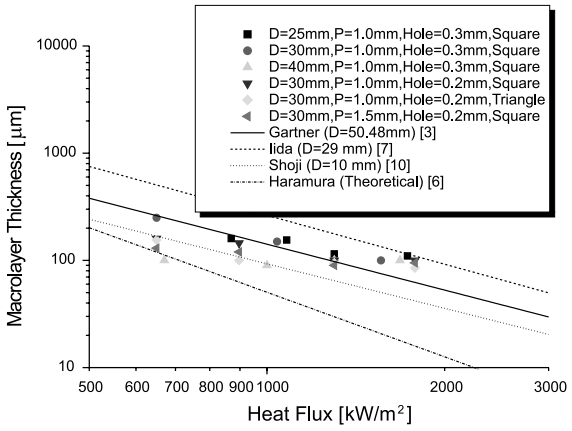

Fig. 12. Behavior of macrolayer thickness with heat flux.

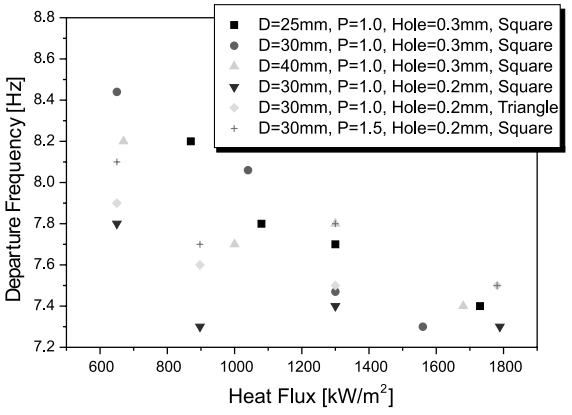

Fig. 13. Bubble departure frequency.

proportional to the applied heat flux, the hovering time increases with the increase in the heat flux. So, the bubble departure frequency is inversely proportional to the heat flux. This agrees with the measured results shown in Fig. 13.

3.3. Estimation of the critical heat flux

From the macrolayer thickness and bubble departure frequency, we can estimate the CHF using Eq. (1), by replacing the term A_v/A_w as the measured void fraction α. Eq. (1) can be rewritten as follows:

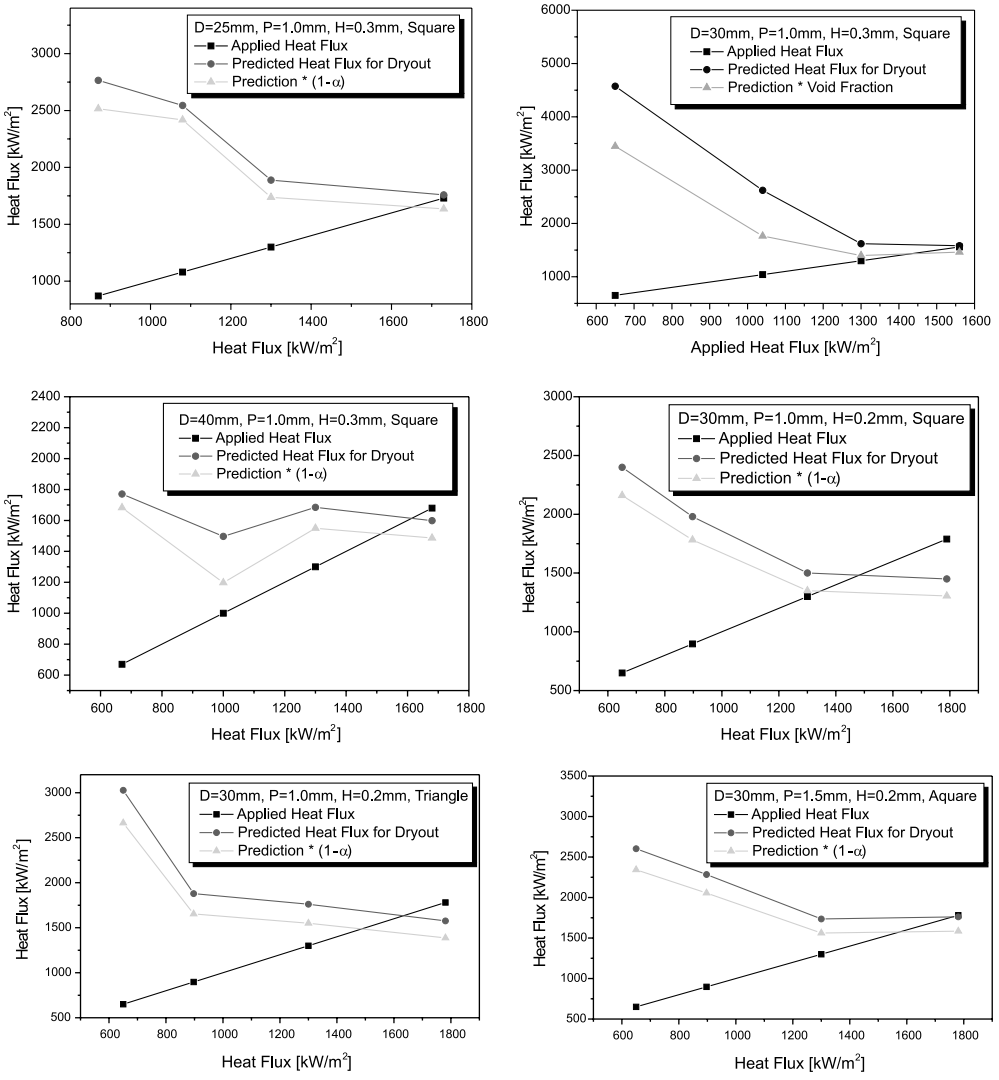

Fig. 14. CHF prediction using macrolayer thickness and bubble departure frequency.

$$q_{\mathrm{CHF}} = \delta_{\mathrm{l}}\rho_{\mathrm{l}}h_{\mathrm{fg}}(1-\alpha)f \tag{7}$$

The estimation of the CHF is illustrated in Fig. 14. Two types of predictions are presented in Fig. 14. The circle represents the prediction neglecting the effect of the void fraction in the liquid macrolayer; that is, the term $(1-\alpha)$ is dropped from Eq. (7). The triangle represents the prediction incorporating the void fraction according to Eq. (7).

As shown in Fig. 14, the difference between the predicted heat flux for dryout and the applied heat flux is reduced as heat flux is approaching to the CHF value. The CHF condition can be determined by the intersection points of two lines. It is noted that the CHF condition can be reasonably established by the present non-boiling tests but further improvements would be required from the quantitative viewpoint.

3.4. The role of non-heating experiments

Through this study, we can propose the non-heating experimental method as a useful alternative for investigating the CHF phenomenon. By the measuring void fraction, the macrolayer thickness and bubble departure frequency from non-heating tests, we can roughly determine the onset of CHF on actual boiling systems.

There is no doubt that the prototypic geometry and fluids should be used in CHF tests as far as possible. However, the prototypic test could be practically impossible in some cases of complex and large geometry,

due to the difficulties in providing reasonable heat flux distributions. In this case, the non-heating experiment can be performed relatively easily to investigate various parametric trends as well as to get the rough estimate of the CHF.

The non-heating experiment with air can simulate only the saturated condition as air bubbles cannot be condensed in water. The difference of physical properties between steam and air also deteriorates the accuracy of the simulation. However, a steam-water system using a steam generator would allow more accurate simulation even for the subcooled condition.

By nature, active nucleation site density varies with the applied heat flux. But, in this methodology, the active nucleation site density is fixed. So, the measured characteristics may be valid at high heat flux conditions with the comparable nucleation site densities.

Despite these limitations, the non-heating method would be a powerful alternative in investigating the CHF mechanisms and parametric effects in both pool and flow boiling, considering the possibility of the relatively easy simulation tests.

4. Conclusions

In this study, a series of non-heating experiments have been conducted to model the CHF in pool-boiling systems. Important findings from this study are summarized as follows:

(a) The measured macrolayer thickness and bubble departure frequency are consistent with previous findings in actual boiling tests.
(b) The measured macrolayer thicknesses are most sensitive to air-blowing rate (heat flux). And, the other parameters cannot give much effect on macrolayer thickness as much as air-blowing rate.
(c) Application of the macrolayer dryout model with the measured values provides reasonable CHF values, confirming the usefulness of the non-heating simulation of the pool-boiling CHF.
(d) The non-heating method with further improvement would be useful in investigating the fundamental mechanisms and parametric effects in both pool and flow boiling involving complex geometries.

Acknowledgements

This work was supported by the Ministry of Science and Technology, Korea, through the National Research Laboratory Program.

References

[1] A.M. Bhat, R. Prakash, J.S. Saini, On the mechanism of macrolayer formation in nucleate boiling at high heat flux, Int. J. Heat Mass Transfer 26 (1986) 735–740.
[2] J.G. Collier, L.R. Thome, in: Convective boiling and condensation, third ed., Clarendon Press, Oxford, 1994, p. 142.
[3] R.F. Gaertner, J.W. Westwater, Population of active sites in nucleate boiling heat transfer, Chem. Eng. Prog. Symp. Ser. 46 (1960) 39–48.
[4] R.F. Gaertner, Photographic study of nucleate boiling on a horizontal surface, ASME J. Heat Transfer 87 (1965) 17–29.
[5] Y. Haramura, Y. Katto, New hydrodynamic model for critical heat flux (CHF), Trans. JSME 49 (1986) 1919–1927.
[6] Y. Haramura, Y. Katto, A new hydrodynamic model of critical heat flux, applicable widely to both pool and forced convection boiling on submerged bodies in saturated liquids, Int. J. Mass Transfer 26 (1983) 389–399.
[7] Y. Iida, K. Kobayashi, An experimental investigation of the effect of subcooling on bubble growth and waiting time in nucleate boiling, ASME J. Heat Transfer 107 (1970) 168–174.
[8] Y. Katto, Y. Yokoya, Mechanisms of burnout and transition boiling in pool boiling, Trans. JSME 37 (1971) 535–545.
[9] D.D. Paul, S.I. Abdel-Khalik, A statistical analysis of saturated nucleate boiling along a heated wire, Int. J. Heat Mass Transfer 26 (1983) 509–519.
[10] M. Shoji, A study of steady transition boiling of water: experimental verification of macrolayer evaporation model, in: Proceedings of the Engineering Foundation Conference on Pool and External Flow Boiling, Santa Barbara, CA, 1992, pp. 237–242.
[11] C.H. Wang, V.K. Dhir, Effect of surface wettability on active nucleation site density during pool boiling of water on a vertical surface, J. Heat Mass Transfer 115 (1993) 659–669.